Journal of Power Sources 270 (2014) 281–291

Contents lists available at ScienceDirect

Journal of Power Sources

journal homepage: www.elsevier.com/locate/jpowsour

A physics based reduced order aging model for lithium-ion cells with phase change

Priya Gambhire [a], Krishnan S. Hariharan [a, *], Ashish Khandelwal [a], Subramanya Mayya Kolake [a], Taejung Yeo [b], Seokgwang Doo [b]

[a] Computational Simulations Group, SAIT-India Lab, Samsung R& D Institute India, Bangalore 560 037, India
[b] Energy Storage Group, Samsung Advanced Institute of Technology, 449-712, Republic of Korea

HIGHLIGHTS

- Reduced order model for cells with phase change electrodes.
- Two phase coexistence described using a concentration dependent diffusivity.
- Easy implementation of degradation to study the cycle life.
- Model captures experimentally observed signatures of phase transition and aging.

ARTICLE INFO

Article history:
Received 5 June 2014
Received in revised form
18 July 2014
Accepted 20 July 2014
Available online 25 July 2014

Keywords:
Lithium ion cells
Phase change electrodes
Lithium iron phosphate
Reduced order model

ABSTRACT

The electrochemical model has the potential to provide a robust and accurate battery management system, but is not the preferred choice as it involves solving non-linear, coupled partial differential equations. In the present work, a model order reduction of the complete electrochemical model for a lithium ion cell with phase change electrodes is carried out. The phase change phenomenon is described using a simple, concentration-dependent diffusivity derived from mixture rules. This reduced order model (ROM) is validated with experimental data from literature. The applicability of the model to capture the atypical behavior of the phase change electrode system is demonstrated. Using the cell response from ROM, charge–discharge asymmetry and path dependence in a lithium iron phosphate (LFP) cell are explored in detail. In addition, side reaction kinetics and solid electrolyte interphase formation are included in the ROM framework to enhance its capability to predict cell aging. The model is used to investigate capacity losses occurring in a phase change electrode cell. Insights from these results are used to suggest cell operating guidelines for maximizing utilization.

1. Introduction

With the advent of alternate energy automobiles such as electric and hybrid electric vehicles, into the commercial market, there is an ever increasing need for a robust Battery Management System (BMS). Within the numerous functions of a BMS, the most important is the accurate prediction of battery state and life. Conventional state estimators make use of equivalent circuit models (ECMs) [1]. In spite of their high speed and accuracy, these state estimators are weighed down by their non-predictive nature and use of a large number of empirical parameters. In the quest for longer lasting batteries, better electrodes involving phase change [2] or engineered composite materials [3] are developed. As ECM based estimators work best within the range of data for which they are tuned, it is difficult to incorporate the atypical behavior inherent to the novel electrode materials using these methods.

Physics based models are more generic than the equivalent circuit models as the processes occurring within the cell are represented accurately in the former. In this context, the electrochemical model (EM) proposed by Doyle et al. [4] is applied to a wide variety of electrochemical systems, including the lithium ion cells. The strength of this approach lies in its applicability to novel electrode materials that show atypical behaviors, like the multiphase coexistence. Intercalation/deintercalation of lithium in certain electrode materials can lead to the formation of one or more new phases. This phase changing property of the electrode most

* Corresponding author.
E-mail address: krishnan.sh@samsung.com (K.S. Hariharan).

http://dx.doi.org/10.1016/j.jpowsour.2014.07.127
0378-7753/

often manifests as a non-monotonic response of the cell voltage. This feature attracts considerable research intrigue and hence is a widely studied area. For certain electrodes such as lithium iron phosphate (LFP) the two phase coexistence results in a constant discharge voltage [2] which holds considerable industrial interest. Widely used negative electrode material, graphite, is also known to transform to a number of phases during cycling [5] adding to the importance of this phenomenon in the electrochemical model.

A variety of approaches are adopted in the literature to include the phase change phenomenon within the electrochemical model. These range from simple physical models which assume the phase formation to be isotropic to complex thermodynamics based models which take into account the anisotropy in phase formation. In one of the pioneering efforts, Srinivasan and Newman [6] represent the new phase formation using the shrinking core physics. Instead of an active material sphere with a single phase, this model assumes a shell and core with the phase boundary at an equilibrium concentration. This approach is applied to model the discharge of an LFP half-cell and an LFP/Carbon (C) full cell [7–9]. The extension of the shrinking core approach to model the charge part of the cycle is proposed via a generalized moving boundary model by Khandelwal et al. [10]. Using this approach, features of the phase transformation in LFP, namely, an asymmetry in the charge and discharge cycles, path dependence of the response and the tangential phase propagation within the LFP material are captured. Motivated by the experimental evidence of anisotropic lithium insertion [11,12], phase field models have been proposed [13–16]. These models are most useful to understand detailed aspects of the phase transformation physics but can prove difficult to translate to onboard algorithms. A major difficulty with the phase change system is to track multiple phase boundaries formed during cell cycling. This is addressed in the generalized moving boundary approach [10] within the shrinking core family of models, while it is obtained as wave solution of the phase field parameter in the phase field family [13] of models, both involving complicated solution schemes.

In an alternate approach, instead of considering a physical boundary, researchers make use of a concentration dependent diffusion coefficient [17,18]. The concentration dependence manifests as a thermodynamic factor/activity correction multiplying the constant diffusion coefficient. But, as electrolyte effects are not considered, this model is applicable only at rates until 1C. Safari and Delacourt [19] also make use of a concentration dependent diffusion coefficient albeit of empirical origin. The advantages of this model include a simplified approach to modeling the phase change whilst considering the highly resistive nature of the LFP material using a resistive-reactant model [20]. The model is validated with experiments on an LFP half-cell [19] and an LFP/C commercial cell [21]. Although the model successfully captures and explains features such as charge–discharge asymmetry and path dependence in LFP, the transport coefficients are obtained by fitting the model results to experiments increasing the dependency on cell data.

A lithium ion cell undergoes degradation from a variety of sources [22]. Electrodes are known to change in volume during the insertion/deinsertion process leading to fatigue and/or cracking while certain positive electrode materials are known to dissolve into the electrolyte [23]. The most common and well-studied mechanism is the occurrence of side reactions within the cell. This involves reduction of the electrolyte at the negative electrode leading to the formation of a Solid Electrolyte Interphase (SEI). The electrochemical model has been used extensively to predict the degradation of lithium ion cells. Studies incorporating just the solvent decomposition reaction [24] or combined with the SEI formation [25] have been carried out in the past. The use of empirical equations to model the capacity loss [26] or the use of first principles based equations describing the SEI growth [27] are incorporated in the aging models. Models predicting calendar life [28] or cycle life [27] of lithium ion cells are also studied. Safari et al. [25] present a multimodal aging model for the lithium cobalt oxide (LCO) cell, valid for cycle life and both constant voltage and OCV storage. In all of the above studies the degradation model is included in one form or the other but is valid for cells with single phase active material electrodes. In terms of modeling the degradation/aging of a phase change electrochemical cell, Safari and Delacourt [29] model the aging of a commercial LFP/C cell. The phase change electrode is modeled using the earlier approach [19] of a concentration dependent diffusivity and the resistive-reactant model. The degradation is included in the form of an SEI evolution equation while considering solvent diffusion as the limiting step to the SEI formation. Although it incorporates phase change, degradation and uses the single particle model approach, the applicability of this model is limited to low and nominal rates as electrolyte effects are not included.

In order to make the electrochemical model amenable for onboard use, it needs to be combined with a certain order reduction methodology. Also, cell aging studies involve long time simulations of the electrochemical degradation models. This proves time consuming for a high number of cycles. Therefore, most often researchers try to incorporate simplified models which can reduce the simulation run time. The single particle model (SPM) proposed by Subramanian et al. [30] and applied by Safari and Delacourt [19] to study degradation of LFP/C cells, is a widely used approach. It is, however, found to be valid only until a current rate of 1C. A number of reduced order models have been proposed by various groups. These reduced order models include but are not limited to the following: enhanced single particle model [31,32], reformulated models [33], state variable models [34] and proper orthogonal decomposition (POD) based models [35]. Of these models, apart from the single particle model, the rest make use of various complicated mathematical techniques for model order reduction. The state variable models need a post processing step such as residue grouping which involves sophisticated mathematics. In addition, the reformulated model and the POD based model require an initial guess of variables and initial data for ensemble, respectively. In the enhanced SPM, the physical basis of the SPM is maintained while the electrolyte effects are included via parabolic [32] or Galerkin approximations [31].

In an alternate approach to reduce the model order, Kumar [36] propose a completely physics based methodology developed using volume averaging. The solid phase equations and the electrolyte profiles are obtained consistently using profile based approximations following the volume averaging. This reduced order model (ROM) approach has a greater range of applicability in terms of current rates, when compared to the SPM and a higher predictability than the numerical model order reduction techniques. On the same lines, Kumar et al. [37] propose an algebraic ROM developed for linearly varying currents motivating that any complicated current profile can be built of smaller linear current segments. These studies are however, confined to single phase electrode cells. Also, prediction of degradation upon cycling or storage is not studied using this model.

A model for a phase change system should incorporate the phenomenon in a simple yet generic way, should be able to predict the cell capacity loss due to aging, should not require extensive tuning to experimental data and should be amenable for onboard implementation in devices. Although the electrochemical model is an ideal approach to predict accurate cell response, to incorporate it in a BMS algorithm a reduced order model is required. The aim of the present work is to develop a physics based reduced order electrochemical model which can predict the response of fresh and

aged cells with phase change active materials. To our knowledge, such a generic ROM incorporating both phase change and degradation has not been carried out. The approach for model order reduction is based on volume averaging and profile based approximations [36]. In the present work, a concentration dependent diffusivity developed from standard mixture rules is used which does not involve any empirical coefficients. The side reaction current is described using the Tafel kinetics and is used in the evolution equation of the SEI film.

The manuscript is structured as follows: The problem description and the model equations are discussed in the following section. Section 3 consists of the results and discussion in which the validation of the fresh as well as aged cell is presented. Following this, the ability of the model to predict the observed atypical behavior of the phase change system is explored. Subsequently, analysis of the LFP/C cell aging is presented. Based on the model results, operating guidelines are proposed to minimize the lithium loss.

2. Model

2.1. Problem description

In the present work a reduced order model is proposed for an LFP/C cell. The model order reduction is along the lines of the methodology proposed by Kumar [36]. A schematic of the cell is given in Fig. 1. To simplify the model and to differentiate the effect of the phase change phenomenon, only the positive electrode is considered to undergo phase change. The negative electrode, under the present range of the lithiation studied, is assumed to have a single phase. The subscripts n, p, 1 and 2 are used to denote the negative electrode, positive electrode, solid phase and the electrolyte phase parameters, respectively. The detailed nomenclature of the variables used is provided in the list of symbols.

2.2. Model equations

The electrochemical model (EM) [4] is based on the concentrated solution theory for porous electrode. The equations used to describe the system consist of mass and charge balances in both the solid phase (electrode) and the electrolyte phase. A list of the governing equations and the corresponding boundary conditions involved in EM are provided in Table 1.

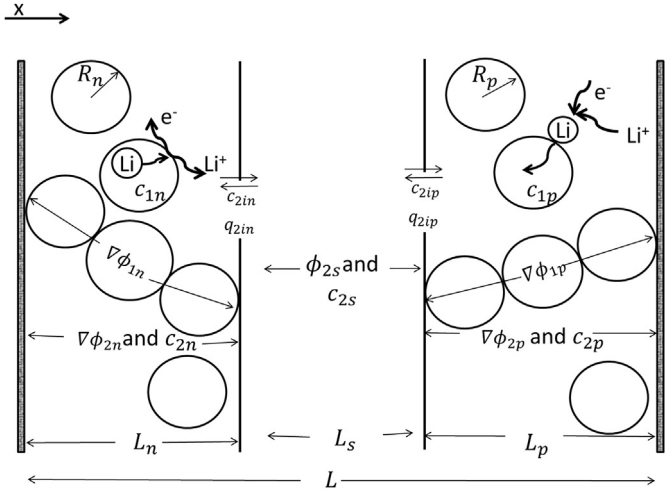

Fig. 1. A schematic representation of the cell.

Table 1
A compilation of governing equations and the boundary conditions used in the complete electrochemical model.

Solid phase mole balance

$\frac{\partial c_{1k}}{\partial t} = \frac{1}{r^2}\frac{\partial}{\partial r}\left(r^2 D_{1k}\frac{\partial c_{1k}}{\partial r}\right)$ where k = n, p

Boundary conditions (BCs)

$-D_{1k}\frac{\partial c_{1k}}{\partial r}\Big|_{r=R_k} = j_k,\ -D_{1k}\frac{\partial c_{1k}}{\partial r}\Big|_{r=0} = 0$

$c_{1k}(r,0) = c_{1k0}$

Solid phase charge balance

$\frac{\partial}{\partial x}\left(-\sigma_{1k}\frac{\partial \phi_{1k}}{\partial x}\right) = -a_k F j_k$

Negative electrode BCs	Positive electrode BCs
$-\sigma_{1n}\frac{\partial \phi_{1n}}{\partial x}\Big\|_{x=0} = I(t)$	$-\sigma_{1p}\frac{\partial \phi_{1p}}{\partial x}\Big\|_{x=L_n+L_s} = 0$
$-\sigma_{1n}\frac{\partial \phi_{1n}}{\partial x}\Big\|_{x=L_n} = 0$	$-\sigma_{1p}\frac{\partial \phi_{1p}}{\partial x}\Big\|_{x=L} = I(t)$

Electrolyte phase mole balance

$\varepsilon_{2k}\frac{\partial c_{2k}}{\partial t} = \frac{\partial}{\partial x}\left(D_{2n}\frac{\partial c_{2k}}{\partial x}\right) + a_n(1-t_+)j_k$

Negative electrode BCs	Positive electrode BCs	Separator BCs
$-D_{2n}\frac{\partial c_{2n}}{\partial x}\Big\|_{x=0} = 0$	$-D_{2p}\frac{\partial c_{2p}}{\partial x}\Big\|_{x=L_n+L_s} = q_{2ip}$	$-D_{2s}\frac{\partial c_{2s}}{\partial x}\Big\|_{x=L_n} = q_{2in}$
$-D_{2n}\frac{\partial c_{2n}}{\partial x}\Big\|_{x=L_n} = q_{2in}$	$-D_{2p}\frac{\partial c_{2p}}{\partial x}\Big\|_{x=L} = 0$	$-D_{2s}\frac{\partial c_{2s}}{\partial x}\Big\|_{x=L_n+Ls} = q_{2ip}$
$c_{2n}\Big\|_{x=L_n} = c_{2in}$	$c_{2p}\Big\|_{x=L_n+L_s} = c_{2ip}$	$c_{2s}\Big\|_{x=L_n} = c_{2in}$
		$c_{2s}\Big\|_{x=L_n+L_s} = c_{2ip}$

Total charge balance (solid + electrolyte)

$-\sigma_{1k}\frac{\partial \phi_{1k}}{\partial x} - \kappa_{1k}\frac{\partial \phi_{2k}}{\partial x} + 2\kappa_{2n}\frac{R_g T}{F}(1-t_+)\frac{\partial \ln c_2}{\partial x} = I$

Negative electrode BCs	Positive electrode BCs	Separator BCs
$-\kappa_{2n}\frac{\partial \phi_{2n}}{\partial x}\Big\|_{x=0} = 0$	$-\kappa_{2p}\frac{\partial \phi_{2p}}{\partial x}\Big\|_{x=L_n+L_s} = I(t)$	$-\kappa_{2s}\frac{\partial \phi_{2s}}{\partial x}\Big\|_{x=L_n} = I(t)$
$-\kappa_{2n}\frac{\partial \phi_{2n}}{\partial x}\Big\|_{x=L_n} = I(t)$	$-\kappa_{2p}\frac{\partial \phi_{2p}}{\partial x}\Big\|_{x=L} = 0$	$-\kappa_{2s}\frac{\partial \phi_{2s}}{\partial x}\Big\|_{x=L_n+Ls} = I(t)$
$\phi_{2n}\Big\|_{x=L_n} = \phi_{2in}(t)$	$\phi_{2p}\Big\|_{x=L_n+L_s} = \phi_{2ip}(t)$	$\phi_{2s}\Big\|_{x=L_n} = \phi_{2in}(t)$
		$\phi_{2s}\Big\|_{x=L_n+L_s} = \phi_{2ip}(t)$

The governing equations are partial differential equations (PDEs), wherein, the dependent variable has both spatial and temporal dependence. To reduce the model order, in the present work, the philosophy followed is to overcome the spatial dependence [36]. The simplest procedure to overcome spatial dependence of variables is to work with their average values. Although, this directly reduces the PDEs to ordinary differential equations this step also leads to loss of spatial information of the system variable. Therefore, the volume averaged variables are coupled with suitable profile approximations to gain back the spatial information. The steps followed are as given below:

To begin with, the average of any system variable $f(x,t)$ across a region of thickness L with a surface area S, in the Cartesian coordinates is defined as,

$$\langle f(t)\rangle = \frac{1}{S\times L}\int_0^L f(x,t)S\mathrm{d}x, \tag{1}$$

where $\langle\ \rangle$ denotes the volume averaged quantity. The average of a variable in the radial coordinates (denoted by an overbar) for a particle of radius R is defined as,

$$\bar{f}(t) = \frac{1}{\frac{4}{3}\pi R^3}\int_0^R 4\pi r^2 f(r)\mathrm{d}r, \tag{2}$$

The primary objective of the model is to estimate the cell voltage which is the potential drop across the positive and the negative electrodes.

$$V_{\mathrm{cell}} = \phi_{1p}\Big|_{x=L} - \phi_{1n}\Big|_{x=0} \tag{3}$$

The solid phase potentials (ϕ_{1p}, ϕ_{1n}) can be calculated from the inverted Butler–Volmer equations,

$$\phi_{1p}|_{x=L} = \phi_{2p}|_{x=L} + U_p(c_{sp}) + \frac{2R_gT}{F}\sinh^{-1}\left(\frac{j_{pi}|_{x=L}}{2j_{p_0}}\right) \quad (4)$$

$$\phi_{1n}|_{x=0} = \phi_{2n}|_{x=0} + U_n(c_{sn}) + \frac{2R_gT}{F}\sinh^{-1}\left(\frac{j_{ni}|_{x=0}}{2j_{n_0}}\right) \quad (5)$$

where, $\phi_{2p}|_{x=L}$ & $\phi_{2n}|_{x=0}$ are the electrolyte phase potentials within the positive and the negative electrodes, at the respective current collector ends and j_{pi} & j_{ni} are the corresponding rates of the intercalation reactions. U_p and U_n are the open circuit potentials of the positive and the negative electrode, respectively, and are functions of the lithium surface concentrations in the electrode particles (c_{sp}, c_{sn}). The surface concentrations are also coupled to the electrolyte phase through the reaction rate prefactors (j_{n0}, j_{p0}) given by,

$$j_{n0} = k_n(c_{1_{maxn}} - c_{sn})^{0.5}c_{sn}^{0.5}c_{2n}^{0.5}, \quad (6)$$

$$j_{p0} = k_p\left(c_{1_{maxp}} - c_{sp}\right)^{0.5}c_{sp}^{0.5}c_{2p}^{0.5}. \quad (7)$$

k_n, k_p are the reaction rate constants, c_{1maxn}, c_{1maxp} are the maximum concentrations within the solid phase and c_{2n}, c_{2p} are the electrolyte phase concentrations, in the negative and positive electrodes respectively.

In the present work, the side reaction involving electrolyte reduction at the negative electrode is considered to be the main source of degradation. The total current at the negative electrode is split into the component responsible for the lithium intercalation/deintercalation reaction and the one responsible for the side reaction. This is explained using a schematic in Fig. 2.

$$\Rightarrow j_n(x,t) = j_{ni}(x,t) + j_s(x,t) \quad (8)$$

The side reaction rate can be modeled using Tafel kinetics [24] as,

$$j_s(x,t) = \frac{-j_{s0}}{F}\exp\left(-\frac{\alpha_c F}{R_gT}\left(\phi_{1n} - \phi_{2n} - U_s - j_n(x,t)R_fF\right)\right). \quad (9)$$

The side reaction results in the formation of a resistive film of reaction products on the electrode surface (SEI). It should be noted

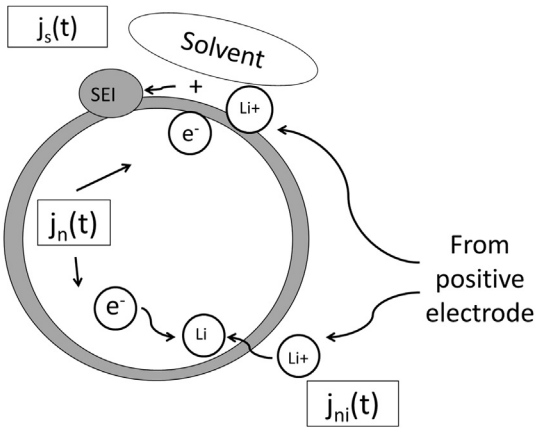

Fig. 2. A schematic representation of the SEI formation on an active material particle surface.

that the overpotential driving the side reaction is affected by the Ohmic drop across this film. The film resistance is calculated as,

$$R_f = R_{f_0} + \frac{\delta_f}{\kappa_f}, \quad (10)$$

where, κ_f is the conductivity of the SEI film while δ_f is the film thickness which is obtained from,

$$\frac{d\delta_f}{dt} = -\frac{j_s M_f}{\rho_f}. \quad (11)$$

That is, evolution of the film depends on its molecular weight (M_f), density (ρ_f) and rate of the side reaction. To take the degradation into account, Eq. (5) is modified to,

$$\phi_{1n}|_{x=0} = \phi_{2n}|_{x=0} + U_n(c_{sn}) + j_n|_{x=0}FR_f|_{x=0} + \frac{2R_gT}{F}\sinh^{-1}\left(\frac{j_n|_{x=0} - j_s|_{x=0}}{2j_{n0}}\right) \quad (12)$$

In the absence of side reaction at the positive electrode, Eq. (4) remains unchanged. In this case, the intercalation reaction current ($j_{pi}(x,t)$) is equal to the total current ($j_p(x,t)$), that is,

$$\phi_{1p}|_{x=L} = \phi_{2p}|_{x=L} + U_p(c_{sp}) + \frac{2R_gT}{F}\sinh^{-1}\left(\frac{j_p|_{x=L}}{2j_{p0}}\right). \quad (13)$$

To determine the cell potential using Eqs. (12) and (13), the unknown variables are the active material surface concentration of lithium and the electrolyte phase potentials at the current collectors. The procedure to obtain these variables is outlined next.

2.2.1. Obtaining the active material surface concentrations

As a first step, the volume averaging procedure given by Eq. (1) is applied to the solid phase charge balance Eq. (refer Table 1) for the negative electrode region. Upon using the boundary conditions, this equation reduces to

$$I(t) = a_nL_nF\langle j_n\rangle(t), \quad (14)$$

where $\langle j_n\rangle$ (t) is the volume averaged reaction flux and $I(t)$ is the applied current. Extending this to the positive electrode and rearranging the equations gives the relation between the average reaction rates and the applied current.

$$\langle j_n\rangle(t) = \frac{I(t)}{a_nL_nF}, \quad (15)$$

$$\langle j_p\rangle(t) = -\frac{I(t)}{a_pL_pF}. \quad (16)$$

The surface concentration of lithium in the active material particles is obtained from the solid phase mass balance equation.

In the present work, the positive electrode active material is considered to undergo phase change during the insertion/deinsertion of lithium. The key step towards modeling a phase change system is to describe the solid phase diffusion accurately. During a major portion of the charge/discharge cycle of the cell, multi phases can coexist. The diffusion within the active material is expected to be affected due to the presence of this coexistence. In the past, the diffusion process has been described using a shrinking-core approach [2,6]. A couple of experimental studies [11,12] of the lithium insertion/deinsertion in LFP materials provide evidence that lithium diffusion occurs preferentially along the *b* direction in the crystal plane and the phase boundary propagates anisotropically throughout the particle. Therefore, solid phase diffusion models with

anisotropic diffusivity [17–19] are studied in lieu of the isotropic shrinking core model. In the present work, this phenomenon is described using a concentration dependent diffusion coefficient developed assuming the system to be a mixture of two phases.

In this regard, the arguments used in the coupling of the pseudo 2D model are applied to this case. In the pseudo 2D model for a porous electrode, it is assumed that the electrode is a homogeneous mixture of both the solid and electrolyte phases. This enables the model to couple the solid phase concentration, obtained by solving the solid mass balance equations (in radial coordinates), to the electrolyte equations, at any point along the thickness of the cell. In a phase change system, irrespective of the mode of the phase boundary propagation, the active material particle consists of the two coexisting phases. A schematic of the arguments presented here is provided in Fig. 3. From the schematic it can be seen that, along the radius of the particle, one encounters a mixture of both the phases.

Accordingly, the diffusivity of the phase change active material particle can be expressed as,

$$D_{1\mathrm{p}_{\mathrm{mix}}} = x_{\mathrm{p}\alpha} D_{1\mathrm{p}\alpha} + x_{\mathrm{p}\beta} D_{1\mathrm{p}\beta} \tag{17}$$

where, $x_{\mathrm{p}\alpha}$, $x_{\mathrm{p}\beta}$ are the mole fractions of the lithium-deficient phase, α and the lithium rich phase, β, respectively and $D_{1\mathrm{p}\alpha}$, $D_{1\mathrm{p}\beta}$ are their diffusion coefficients. $x_{1\mathrm{p}\alpha}$ and $x_{1\mathrm{p}\beta}$ are given by the following equations,

$$x_{1\mathrm{p}\alpha} = \frac{c_{1\mathrm{p}\beta} - \langle c_{1\mathrm{p}} \rangle}{c_{1\mathrm{p}\beta} - c_{1\mathrm{p}\alpha}} \tag{18}$$

$$x_{1\mathrm{p}\beta} = 1 - x_{1\mathrm{p}\alpha} \tag{19}$$

It can be noted that the diffusivity varies with the average concentration, $c_{1\mathrm{p}}$ while taking into account the equilibrium concentrations and diffusivities of the individual phases (α and β) present in the system. When $c_{1\mathrm{p}}$ is equal to either $c_{1\mathrm{p}\alpha}$ or $c_{1\mathrm{p}\beta}$, the diffusion coefficient is equal to the pure phase diffusivity, $D_{1\alpha}$ and $D_{1\beta}$, respectively.

The solid phase mass balance for the positive electrode undergoing phase change can be written as

$$\frac{\partial c_{1\mathrm{p}}}{\partial t} = \frac{1}{r^2}\frac{\partial}{\partial r}\left(r^2 D_{1\mathrm{p}_{\mathrm{mix}}} \frac{\partial c_{1\mathrm{p}}}{\partial r}\right) \tag{20}$$

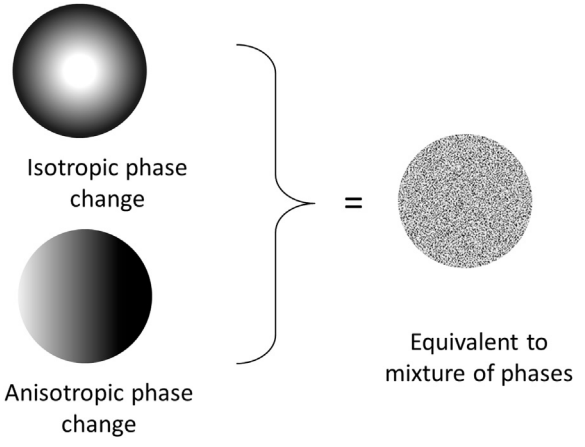

Fig. 3. A schematic representation of the isotropic shrinking core approach and the anisotropic phase propagation approach adopted for a phase change system in literature. Irrespective of the model of phase formation, in the present work, the system is considered to be equivalent to a mixture of two phases.

$$\text{With the BCs}: \quad -D_{1\mathrm{p}_{\mathrm{mix}}} \frac{\partial c_{1\mathrm{p}}}{\partial r}\Big|_{r=R_{\mathrm{p}}} = j_{\mathrm{p}i}, \quad -D_{1\mathrm{p}_{\mathrm{mix}}} \frac{\partial c_{1\mathrm{p}}}{\partial r}\Big|_{r=0} = 0 \tag{21}$$

while that for the negative electrode undergoing degradation is given by

$$\frac{\partial c_{1\mathrm{n}}}{\partial t} = \frac{1}{r^2}\frac{\partial}{\partial r}\left(r^2 D_{1\mathrm{n}} \frac{\partial c_{1\mathrm{n}}}{\partial r}\right) \tag{22}$$

$$\text{With the BCs}: \quad -D_{1\mathrm{n}} \frac{\partial c_{1\mathrm{n}}}{\partial r}\Big|_{r=R_{\mathrm{n}}} = j_{\mathrm{n}i}, \quad -D_{1\mathrm{n}} \frac{\partial c_{1\mathrm{n}}}{\partial r}\Big|_{r=0} = 0 \tag{23}$$

Applying the volume averaging [30] given by Eq. (2) to the solid phase mole balance Eqs. (20) and (22) and using the boundary conditions, leads to the equation,

$$\frac{\mathrm{d}\bar{c}_{1\mathrm{k}}}{\mathrm{d}t} = -\frac{3 j_{\mathrm{k}i}}{R_{\mathrm{k}}}, (\mathrm{k} = \mathrm{n}, \mathrm{p}) \tag{24}$$

It can be noted that the above equation gives the concentration of lithium averaged over one single particle. This equation is, therefore, subjected to averaging across the electrode volume Eq. (1) to obtain,

$$\frac{\mathrm{d}\langle \bar{c}_{1\mathrm{k}} \rangle}{\mathrm{d}t} = -\frac{3\langle j_{\mathrm{k}i} \rangle}{R_{\mathrm{k}}} \tag{25}$$

The average reaction rate $\langle j_{\mathrm{k}i} \rangle$ is equal to $\langle j_{\mathrm{p}} \rangle(t)$ for the positive electrode and can be replaced by the relation to the applied current given by Eq. (16). For the negative electrode, the relation given by Eq. (8) is used to obtain the relation with the total current.

To obtain the concentration gradient within the active material particle, the quartic profile described by Subramanian et al. [30] and Kumar [36] is found to be most suitable. Following the procedure outlined therein, the radial gradient of the lithium within the active materials can be obtained by solving,

$$\frac{\mathrm{d}\bar{c}_{1\mathrm{kr}}}{\mathrm{d}t} = -\frac{30 D_{1\mathrm{k}} \bar{c}_{1\mathrm{kr}}}{R_{\mathrm{k}}^2} - \frac{45 j_{\mathrm{k}i}}{2 R_{\mathrm{k}}^2} \tag{26}$$

wherein, $D_{1\mathrm{k}} = D_{1\mathrm{p}_{\mathrm{mix}}}$ for the positive electrode and is given by Eq. (17). These equations upon solving can be used to obtain the surface concentrations in both the electrodes

$$c_{\mathrm{s}_{\mathrm{k}}} = \bar{c}_{1\mathrm{k}} - \frac{R_{\mathrm{k}} j_{\mathrm{k}i}}{35 D_{1_{\mathrm{k}}}} + \frac{8 R_{\mathrm{k}} \bar{c}_{1\mathrm{kr}}}{35} \tag{27}$$

2.2.2. Obtaining the electrolyte phase potentials

To obtain the electrolyte phase potentials at the current collector ends, the total charge balance listed in Table 1 is used. This equation includes contribution from the solid phase charge balance and is coupled with the electrolyte phase concentration.

To take into account the spatial variation of the solid phase potential ($\phi_{1\mathrm{k}}$), the local reaction rate is assumed to be equal to its volume average value.

$$j_{\mathrm{k}}(x,t) \sim \langle j_{\mathrm{k}} \rangle(t) (\mathrm{k} = \mathrm{n}, \mathrm{p}), \tag{28}$$

Substituting the value of average reaction rate instead of the local in the solid phase charge balance, integrating and applying the electrode–electrolyte interface boundary condition leads to the expression for the electric field in the solid phase of the electrodes.

$$-\sigma_{1\mathrm{n}} \frac{\partial \phi_{1\mathrm{n}}}{\partial x} = -\frac{I(t)}{L_{\mathrm{n}}}(L_{\mathrm{n}} - x) \tag{29}$$

$$-\sigma_{1p}\frac{\partial\phi_{1p}}{\partial x} = \frac{I(t)}{L_p}(x-(L_n+L_s)) \tag{30}$$

The concentration within the electrolyte is obtained by solving the electrolyte phase mass balance equations in the electrodes and separator. The volume averaged forms of the equations are obtained by using Eq. (1) and the flux boundary conditions to be,

$$L_n\varepsilon_{2n}\frac{d\langle c_{2n}\rangle}{dt} = -q_{2in} + (1-t_+)a_nL_n\langle j_n\rangle \tag{31}$$

$$L_p\varepsilon_{2p}\frac{d\langle c_{2p}\rangle}{dt} = q_{2ip} + (1-t_+)a_pL_p\langle j_p\rangle \tag{32}$$

$$L_s\varepsilon_{2s}\frac{d\langle c_{2s}\rangle}{dt} = q_{2in} - q_{2ip} \tag{33}$$

In order to obtain the concentration profiles within the electrolyte phase, the local value of the gradient of diffusive concentration flux (within the electrolyte) is substituted with its average value.

$$\frac{\partial}{\partial x}\left(D_{2k}\frac{\partial c_2}{\partial x}\right) = -\frac{q_{2ik}}{L_k} \tag{34}$$

In Eq. (34), k takes the values n and p for the negative and the positive electrode, respectively. Integrating these equations in both the electrodes and the separator regions whilst using the concentration boundary conditions, the electrolyte phase concentrations are obtained as

$$c_{2n}(x,t) = c_{2in}(t) + \frac{q_{2in}(t)}{2L_nD_{2n}}\left(L_n^2 - x^2\right) \tag{35}$$

$$c_{2p}(x,t) = c_{2ip}(t) - \frac{q_{2ip}(t)}{2L_pD_{2p}}\left(L_p^2 - (L-x)^2\right) \tag{36}$$

$$c_{2s}(x,t) = c_{2in}(t) - \frac{q_{2in}(t)}{D_2p}(x-L_n) + \left(\frac{q_{2in}(t)-q_{2ip}(t)}{L_sD_{2s}}\right)\frac{(x-L_n)^2}{2} \tag{37}$$

where, c_{2in}, c_{2ip}, q_{2in} and q_{2ip} are concentration and flux variables at the electrode–electrolyte interface. They are determined by summation of the total concentration in the electrolyte phase and can be obtained from Eqs. (83), (84), (78) and (79) in Kumar [36].

Knowing the concentration profiles (Eqs. (35)–(37)) and the relation between the electric field in the solid phase and the applied current (Eqs. (29) and (30)), the total charge balance is integrated to obtain the electrolyte phase potentials. At the current collector ends the values are,

$$\phi_{2n}\big|_{x=0} = \phi_{2in} + \frac{2R_gT}{F}(1-t_+)\log\left(\frac{c_{2n}(x=0)}{c_{2in}}\right) + \frac{IL_n}{2\kappa_{2n}} \tag{38}$$

$$\phi_{2p}\big|_{x=L} = \phi_{2ip} + \frac{2R_gT}{F}(1-t_+)\log\left(\frac{c_{2p}(x=L)}{c_{2ip}}\right) + \frac{IL_p}{2\kappa_{2p}} \tag{39}$$

Using Eqs. (27), (38) and (39) in Eqs. (6), (7), (12) and (13), the solid phase potentials at the current collector ends are obtained. These are used to obtain the cell response using Eq. (3).

To summarize the discussion of the model equations, the complete electrochemical model for a cell with a phase change positive electrode, with degradation, is reduced to solving ordinary differential equations and algebraic equations. These equations are incorporated in Simulink through a Matlab function block. The differential equations are solved using integrator blocks which uses the ODE15s solver. A discussion of the results is provided in the next section.

3. Results and discussion

In the present section, the results from ROM, which includes multiphase behavior of electrode materials and a kinetic SEI growth model to study the cycle life of cells, are presented. The first part deals with the discussion of fresh cell results followed by the cell aging studies.

3.1. Model validation

3.1.1. Reduced order model for phase change system (j_s ~ 0)

To demonstrate its validity, ROM for fresh cells (first cycle) is compared to experimental data from literature. Safari and Delacourt [21] report galvanostatic charge–discharge curves at different rates for an LFP/C cell. For the present work, data points for two rates namely, C/10 and 1C are used for model validation. The values of the cell parameters used are same as those reported by Ye et al. [38], Safari and Delacourt [21] and are listed in Table 2. A comparison of model results with experimental data is shown in Fig. 4. Good agreement between the experimental and simulated values is observed, especially at the beginning and end of the charge/discharge cycles. A relative mismatch is observed in the mid portion of the curves. This mismatch is seen to be higher during discharge than during the charge cycle. It is also found to be increasing with rate but the extent of mismatch is found to be less than 1.8%. This substantiates the utility of this phase change reduced order model at both low and nominal rates.

3.1.2. Reduced order model for phase change system with degradation

To study the degradation of LFP/C cell, the side reaction rate is assumed to have a finite value during the charging cycle. Safari and Delacourt [39] report experimental cell response data for various cycles for an LFP/C cell. As the initial states ($SOC_0 = c_{10}/c_{1max}$) for these set of experiments are different, the values of $SOC_{n0} = 0.79$, $SOC_{p0} = 0.03$ are used for validating the cycling results. A comparison of model results with experimental data for the first and

Table 2
A list of the parameters used in the model.

S. no	Parameter	$LiFePO_4$	LiC_6	Separator	Source
1	L (m)	70×10^{-6}	34×10^{-6}	30×10^{-6}	[38]
2	r (m)	36.5×10^{-9}	3.5×10^{-6}		[38]
3	ε_2	0.332	0.33	0.54	
4	ε_1	0.43	0.55		
5	D_1 ($m^2\ s^{-1}$)	Eq. (17)	3.9×10^{-14}		[38]
6	D_2 ($m^2\ s^{-1}$)			2.8×10^{-10}	[38]
7	c_{1max} (mol m^{-3})	22,806	31,370		[38]
8	c_{10}/c_{1max}	0.035	0.82		
9	c_{20} (mol m^{-3})		1200		
9	k (m s^{-1})	1.4×10^{-12}	8.19×10^{-12}		[38]
10	κ (S m^{-1})	1.3634	1.3459	1.3566	[38]
11	S (m^2)	0.1694	0.1755		

S. no	Parameter	SEI film	Source
1	j_{s0} (mol $m^{-3}\ s^{-1}$)	$3.4\times10^{-11}\times0.05\times4.541$	[29]
2	ρ_f (kg m^{-3})	1690	[29]
3	M_f (kg mol^{-1})	0.162	[29]
4	κ_f (S m^{-1})	3.8×10^{-7}	[29]
5	U_s (V)	0.38	[29]

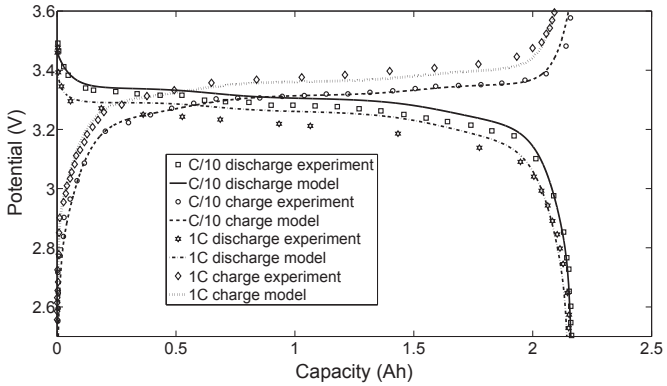

Fig. 4. The model results are validated with the experimental data reported in Safari and Delacourt [21] at different rates for both charge and discharge cycles.

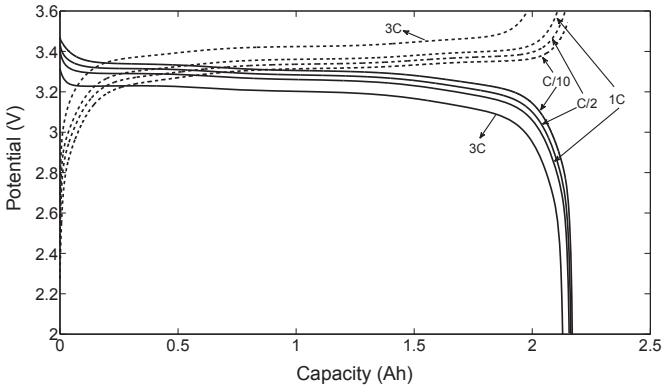

Fig. 6. Charge and discharge curves at different rates are plotted for the LFP/C cell under study. An asymmetry in the end capacities is observed.

the 310th cycle is given in Fig. 5. An excellent match between the model and experimental results with <1% error is observed. This benchmarks the ROM approach used in the present work to model degradation of a phase change cell and demonstrates the applicability of the model.

3.2. Charge–discharge asymmetry

Due to multi-phase coexistence, an interesting feature of LFP/C cells is the charge–discharge asymmetry. In Fig. 4, an asymmetry in the end capacities (utilization) during charge and corresponding discharge cycle, is observed. To explore this observation further, rate capability results for the fresh LFP/C cell are studied. Assuming a completely charged initial state, the cell discharge at four different rates is shown (solid lines) in Fig. 6. At the same rates, the cell response during charge from a completely discharged state is shown as dashed lines. At low rates, say C/10, the end capacity for discharge and charge are the same. While the end capacities do not vary significantly during discharge, the decrease in the end capacities during charge is quite significant. This gives rise to an asymmetry in the charge and discharge profiles. This asymmetric behavior is characteristic of the phase change electrode and has been reported previously [10,19]. Thus it is observed that the proposed model can be used to characterize the observed atypical features of phase change cells.

In Fig. 7 the end capacities obtained during charge and discharge are plotted as a function of the current rate. It is observed that at any particular rate, the end capacity obtained via charging is lower than that obtained via discharging. The difference in the end capacities is found to increase with increasing rate. The feature is observed in experiments by Safari and Delacourt [21].

To understand the asymmetry further, concentration profiles during charge and discharge, within the positive electrode, are investigated. The evolution of the average concentration for a 1C discharge is shown in Fig. 8 as a solid line, while that during charge is given by a dashed line. It is observed that the change in the concentration during charge and during discharge is the same, but, the time taken to do so, and hence the capacity, is different. The asymmetric response is attributed to the different values of transport coefficients between charge and discharge [40]. In the shrinking core approach [6,10] this is taken into account by considering different diffusivities of the α and β phases. The present model accounts for the same behavior by the concentration dependent diffusion coefficient (Eq. (17)).

3.3. Path dependence

The heterogeneous environment in the active material particle, due to the coexistence of two phases, affects the transport of lithium during insertion differently than during deinsertion. For example, for LFP during discharge, a lithium rich phase (β) forms at the cost of the initial lithium poor phase (α) and the reverse occurs during the charge cycle. As the diffusion coefficients are different for these two phases [40], lithium transport correspondingly takes shorter or longer depending on the phase it travels through.

A complete and accurate prediction of path dependence of a cell is an important requirement for building the BMS [40]. This feature

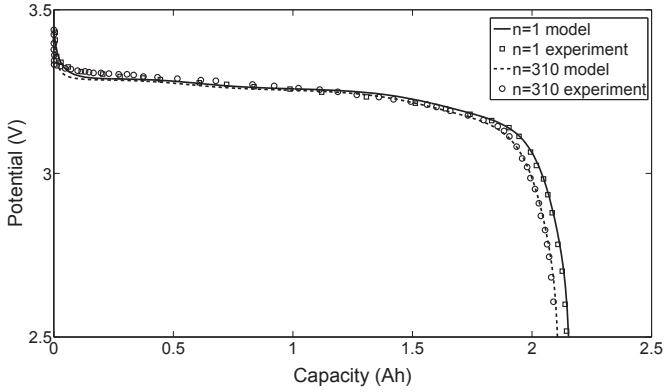

Fig. 5. The model results are validated with the cycle life experimental data reported in Safari and Delacourt [39] at different discharge cycles.

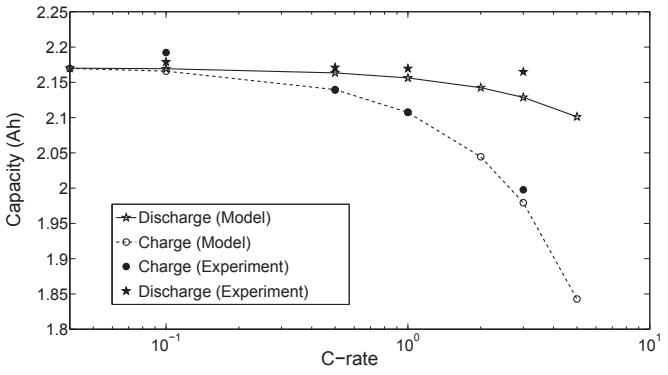

Fig. 7. The end capacities of the charge and discharge curves in Fig. 6 are plotted as a function of the current rates.

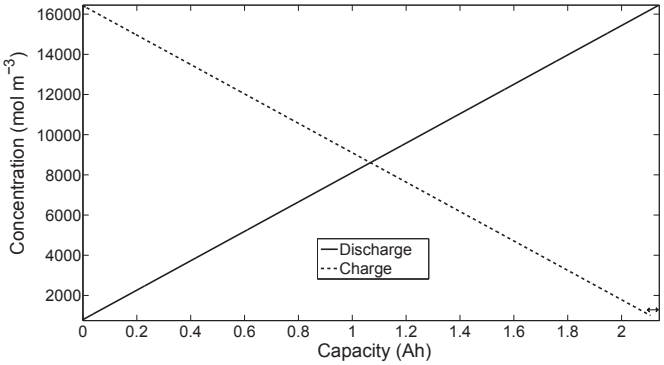

Fig. 8. The average concentration of the two phase system varying during discharge and charge. The mismatch in the end concentrations is indicated by the arrow.

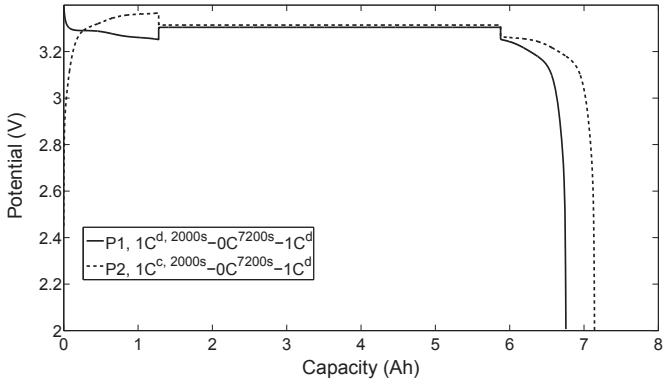

Fig. 9. The simulated response of the LFP/C cell to two different current paths.

has earlier been explained using the shrinking core model [40] and the generalized moving boundary model [10]. These models have phase boundaries defined which specify the diffusion lengths involved in different paths. In the present work, in order to make the model amenable for multi-cycling studies, no explicit phase boundary is considered. It is therefore interesting to study if the path dependence can be captured by the present description of the phase change system.

To demonstrate the model's capability in predicting the path dependent behavior of the phase change cell (LFP/C), two different protocols are used. In the first protocol, the time for the different paths is fixed allowing the concentration to vary while in the second protocol, the concentration to be attained at the end of the path is fixed.

3.3.1. Fixed time protocol

In the fixed time protocol to study path dependence, the response of the cell subjected to two different paths is compared. In the first path (P1), the cell is discharged from a completely charged state for 2000 s. This forms the first stage of the path. In the second stage it is let to rest for 2 h. This long rest period ensures that the cell is equilibrated. In the third stage, post resting, the cell is discharged until it reaches the cut-off voltage of 2 V. The second path (P2) differs from P1 only in the first stage, wherein, the cell is charged from a completely discharged state for 2000 s. The following two stages, the rest and discharge steps, remain same as those in P1. The details of the paths are summarized in Table 3. The cell potential for the complete path is plotted as a function of the cell capacity in Fig. 9. Irrespective of the initial stages, in both the cases, the cell is rested for two hours, yet, a clear difference in the end capacities is observed. The discharge curve of P2, with an initial charging stage, is found to have a higher end capacity than the other.

To gain a physical understanding of the path dependence, the average concentration of lithium in the active material particles, for both the paths, is plotted as a function of the cell capacity in Fig. 10. It can be seen from the figure, at the beginning of the stage 3, that the average concentration in the cell while undergoing P1 is higher than when undergoing P2. This mismatch is the result of the asymmetry in the charge discharge utilization as discussed in the Section 3.2. This in turn, leads to an asymmetry in the end capacities originating from the initial paths taken.

Table 3
A summary of the various paths used in the present work, to study the path dependence in LFP/C cells.

Path	Stage 1	Stage 2	Stage 3	Result
Fixed time protocol				
P1	1C, $t = 2000$ s	0C, $t = 7200$ s	1C, $V_{cutoff} = 2$ V	Lower utilization
P2	−1C, $t = 2000$ s	0C, $t = 7200$ s	1C, $V_{cutoff} = 2$ V	
Fixed concentration protocol				
P1	1C, SOC = 0.5	0C, $t = 7200$ s	1C, $V_{cutoff} = 2$ V	
P2	−1C, SOC = 0.5	0C, $t = 7200$ s	1C, $V_{cutoff} = 2$ V	Lower utilization
P3	−1C, SOC = 0.5	0C, $t = 7200$ s	−1C, $V_{cutoff} = 3.5$ V	
P4	1C, SOC = 0.5	0C, $t = 7200$ s	−1C, $V_{cutoff} = 3.5$ V	Lower utilization

3.3.2. Fixed concentration protocol

In this protocol, the cell is subjected to four different paths. As in the earlier protocol, all the paths involve three stages. In the first path (P1), the first stage involves discharging the cell to a state of charge (where SOC = c_{sp}/c_{1max_p}) of 0.5. That is, instead of fixing the time as done in section (3.3.1), the concentration to which the cell is discharged is fixed. In the second stage, the cell is rested for 2 h followed by a third stage, wherein, the cell is discharged from this state to a cut off voltage of 2 V. The second path (P2), differs from the first path only in the first stage. In P2, the cell is charged from a completely discharged state to SOC = 0.5 followed by a 2 h rest and 1C discharge to 2 V. Path 3 (P3) is the reverse of P1. In the first stage of P3, the cell is charged from a completely discharged state to SOC = 0.5. This is followed by rest for 2 h and 1C charging to a cut-off voltage of 3.5 V. The fourth path (P4) differs from P3 only in the first stage. It involves a discharge to the mid SOC followed by rest and then charge to the cut-off of 3.5 V. The details of the paths are summarized in Table 3. The response of the cell to all the four paths is plotted in Fig. 11. As the mid SOC is reached at different times during charging and discharging, the cell response ends at different times. To exclude this effect, the time after rest, that is, the beginning of the stage 3 for all the four paths is considered to be initial time ($t = 0$) in the inset of the same figure.

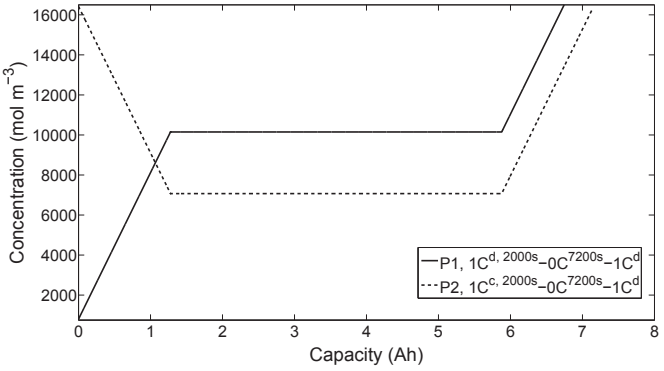

Fig. 10. The variation of the average concentration of the lithium in the positive electrode during the paths 1 and 2.

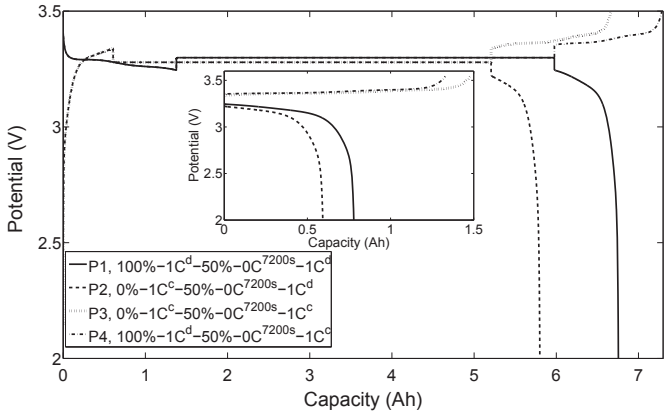

Fig. 11. The simulated response of the LFP/C cell to two different current paths.

From the inset in Fig. 11, a capacity loss in both the discharge and the charge cycles can be observed. Within the discharge curves (P1 and P2), the curve which has a history of a charge cycle (P2) shows a lower utilization while within the charge curves (P3 and P4), the path (P4) with a history of a discharge cycle shows a lower utilization.

To understand the origin of this path dependence, the surface and average concentrations in the positive electrode particles are plotted as a function of the cell capacity for the two discharge paths P1 and P2 in Fig. 12. From the figure, it can be noticed that at the end of the stage 1, the surface concentrations reach $0.5 \times c_{1\max_p}$ but upon resting in stage 2 they relax to different average concentrations. These average concentrations form the initial state for the stage 3. As the stage 3 in the P1 begins with a lower concentration, the corresponding diffusion coefficient is higher resulting in better lithium transport and higher utilization.

Above discussion leads to following observations: Partial charging of phase change cells from a completely discharged state, before use (discharge), can lead to lower utilization. On the same lines paths 3 and 4 suggest that while charging, higher capacity can be attained if the preceding stage is charging. That is, lower utilization can occur when charging a partially discharged cell. The analysis of the model results show that the utilization can be maximized if similar stages (charge or discharge) succeed one another. The insights from this path dependence study can be used as operating guidelines for cells such as LFP/C that exhibit phase change.

3.4. Cycle life

In this section, cycle life of the LFP/C cell is studied. As discussed in Section 2, the cell degrades due to side reactions occurring on the

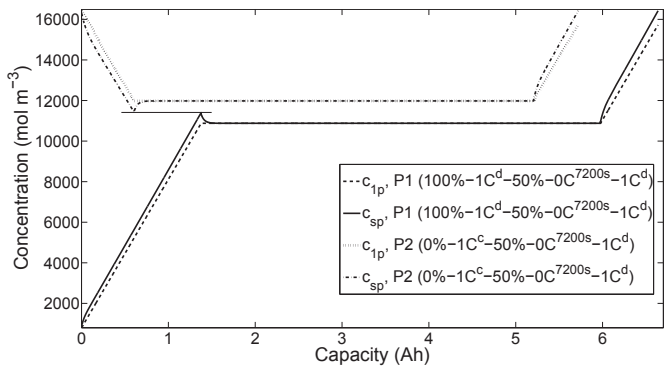

Fig. 12. The surface and average concentrations within the positive electrode of the LFP/C cell varying due to two different current paths.

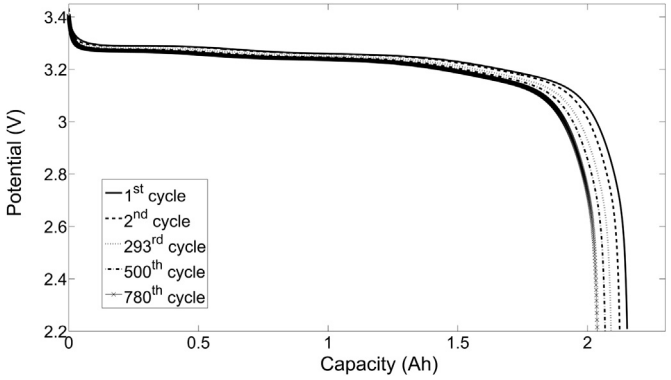

Fig. 13. The discharge curves of the LFP/C cell at different cycles.

negative electrode surface during aging. The reaction consumes lithium ions causing capacity loss while the products form an SEI film on the active material particle surface increasing the cell resistance while in operation. The proposed model has been validated with experimental data from the literature in Section 3.1.2. The discharge curves at different cycles are plotted in Fig. 13. A loss in capacity is observed immediately after the first cycle indicating the formation of SEI film. The film grows with time increasing the resistance which manifests as voltage drop with increasing cycle number. The increase in resistance however lowers the overpotential for side reaction which slows the growth of the film. This leads to a continuous albeit slower loss in capacity with increasing cycle numbers.

The SEI film thickness as a function of time is presented in Fig. 14. The film growth is found to be linearly increasing with the cycling time and hence, in extension, it is linear with the number of cycles. Broussely et al. [41] study the aging of lithium ion cells under various operation regimes. In the regime where the conductivity of the SEI film becomes rate controlling, they propose a linear scaling between the SEI film growth and the number of cycles. In the present work, the SEI film influences the cell potential through an Ohmic drop across it. That is, the overpotential driving the electrochemical reaction is directly affected by the film resistance. Therefore, the scaling law provided by Broussely et al. [41] corroborates the linear film growth observed in the present work. This provides a consistency check for the description of degradation used in the model.

3.4.1. Rate dependence

The results from the ROM degradation model are used to study the rate dependence of the SEI film growth. For a fixed number of

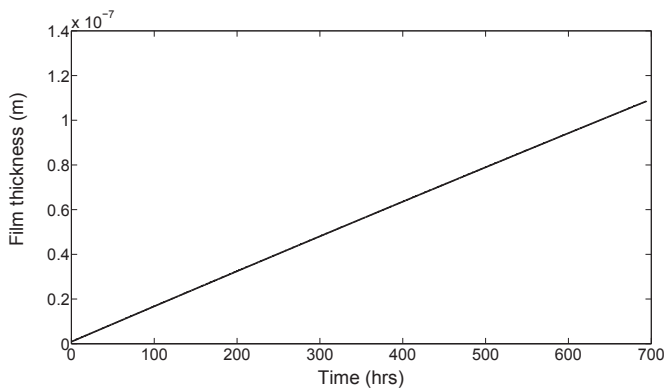

Fig. 14. The growth of the SEI film as a function of the cycling time in hours.

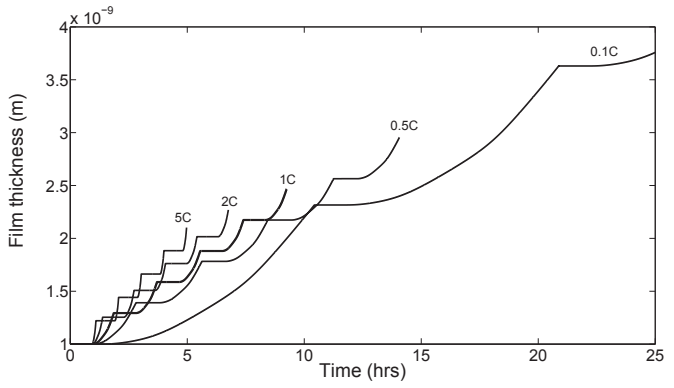

Fig. 15. The growth of the SEI film varying as a function of the current rate for a fixed number of cycles.

cycles, the increase in the SEI film thickness is plotted as a function of the current rate in Fig. 15. As the SEI formation occurs during the charge cycle, the charge rate is varied while keeping the discharge rate constant at 1C. From Fig. 15, it can be observed that for a fixed number of cycles the SEI growth decreases with increase in the charge rate. At 5C, the SEI growth at the end of 5 cycles is almost equal to the growth observed in a single charge cycle at 0.1C.

This rate dependence of the SEI film thickness originates from an interplay of the side reaction rate and the time available for its growth. At higher current rates, a constant current charge cycle occurs in 1/5th of the time it would take at 1C. This gives lesser time for the side reaction to occur and hence leads to lower SEI film growth.

For high power applications low cell resistance is preferred. This translates to minimal SEI growth during the operation. While for high energy applications, to avoid continuous loss of lithium to the side reactions, formation of a stable SEI in the first cycle followed by a quick saturation in its growth is preferable. The insights from the present model results can be used to design suitable charging profiles. For example, incorporating a higher rate constant current charging segment can lead to a lower SEI growth for a high power cell. While a lower rate constant current charging can lead to a rapidly saturating first cycle SEI growth for a high energy cell.

3.5. Operating guidelines

In the previous sections, the implication of the phase change phenomenon on the fresh and aged cell response is discussed. The features observed as a result of the two-phase coexistence are used to suggest the following operating guidelines for maximizing utilization of cells such as LFP/C

- For a fresh cell, utilization can be maximized if similar stages (charge or discharge) succeed one another.
- To obtain a lower SEI growth (suitable for power cells) a higher rate constant current charging segment can be incorporated.
- For a saturated SEI film (suitable for energy cell) a lower rate constant current charging is recommended which can lead to a rapidly saturating first cycle SEI growth.

4. Conclusion

A physics based reduced order model (ROM) is proposed for lithium ion cells with a phase change electrode. A simple and novel approach is adopted to model the multi-phase coexistence within the active material using a concentration dependent diffusivity. The proposed ROM is validated against experimental data from literature. It is demonstrated that the model can exhibit the characteristic experimental behavior of the phase change electrodes. It is also used to gain physical insight into various features of a phase change system such as charge discharge asymmetry and path dependence. As the model innately takes into account the formation of multiple phases it enables studying the cycle life of cells with phase change electrodes. To this end, the effect of SEI formation due to side reactions is implemented in this ROM framework and validated with experimental data. It is demonstrated that higher rates of constant current charging lead to lower film formation. Optimum operating protocols which can reduce either the capacity or the voltage losses can be obtained using this reduced order model. To conclude, the present ROM based on physical principles can be used for BMS applications due to its algorithmic structure. It can also be used to obtain physical insights into the electrochemical processes leading to optimum utilization of the cell. Additional physics such as thermal effects can easily be adopted into this framework which forms the scope of future work.

Acknowledgment

The authors would like to acknowledge V. Senthil Kumar for his contribution in deriving the effective mixture diffusion coefficient.

List of symbols

a	specific surface area of the porous active material, m^{-1}
c	concentration of lithium, mol m^{-3}
c_s	surface concentration of lithium, mol m^{-3}
D	diffusion coefficient of lithium, m^2 s^{-1}
F	Faraday's constant, C mol^{-1}
i	current density, A m^{-2}
I	total current density, A m^{-2}
L	thickness of the electrode/separator/cell, m
k	reaction rate, m s^{-1}
j	reaction rate at the pore wall interface, mol m^{-2} s^{-1}
M	molecular weight of the SEI film, kg mol^{-1}
q	mass flux at the electrode–electrolyte interface, mol m^{-2} s^{-1}
r	radial coordinate, m
R	radius of the active particle within the electrode, m
R_g	Ideal gas constant, J (mol K)$^{-1}$
R_f	SEI film resistance, Ω m^2
S	surface area of the electrode, m^2
t_+	transference number of the lithium ions
t	time, s
T	temperature, K
U	open circuit voltage, V
V	cell voltage, V
x	Cartesian coordinate
α_c, α_a	charge transfer coefficients
δ	SEI film thickness, m
ε	porosity
κ	electrical conductivity of the electrolyte phase, S m^{-1}
ρ	density of SEI film, kg m^{-3}
σ	electrical conductivity of the solid phase, S m^{-1}
ϕ	potential, V

Subscript

f	film variable
in, ip	interfacial variables
max	maximum value of the variable
n	negative electrode properties
ni, pi	intercalation reaction

p	positive electrode properties
s	side reaction variable
0	initial value of the parameter
1	solid phase properties
2	electrolyte phase properties
α	lithium deficient phase
β	lithium rich phase

References

[1] H. He, R. Xiong, J. Fan, Energies 4 (2011) 582–598.
[2] A.K. Padhi, K.S. Nanjundaswamy, J.B. Goodenough, J. Electrochem. Soc. 144 (4) (1997) 1188–1194.
[3] C.H. Chen, J. Liu, M.E. Stoll, G. Henriksen, D.R. Vissers, K. Amine, J. Power Sources 128 (2004) 278–285.
[4] M. Doyle, T.F. Fuller, J. Newman, J. Electrochem. Soc. 140 (6) (1993) 1526–1533.
[5] T. Ohzuku, Y. Iwakoshi, K. Sawai, J. Electrochem. Soc. 140 (9) (1993) 2490–2498.
[6] V. Srinivasan, J. Newman, J. Electrochem. Soc. 151 (10) (2004) A1517–A1529.
[7] Q. Zhang, R.E. White, J. Electrochem. Soc. 154 (6) (2007) A587–A596.
[8] C. Wang, U.S. Kasavajjula, P.E. Arce, J. Phys. Chem. C 111 (2007) 16656.
[9] S. Dargaville, T.W. Farrell, J. Electrochem. Soc. 157 (7) (2010) A830–A840.
[10] A. Khandelwal, K.S. Hariharan, V.S. Kumar, P. Gambhire, S.M. Kolake, D. Oh, S. Doo, J. Power Sources 248 (2014) 101–114.
[11] G. Chen, X. song, T.J. Richardson, Electrochem. Solid-State Lett. 9 (6) (2006) A295–A298.
[12] C. Delmas, M. Maccario, L. Croguennec, F.L. Cras, F. Weill, Nat. Mater. 7 (2008) 665–671.
[13] G.K. Singh, G. Ceder, M.Z. Bazant, Electrochim. Acta 53 (2008) 7599–7613.
[14] D. Burch, G. Singh, G. Ceder, M.Z. Bazant, Solid State Phenom. 139 (2008) 95–100.
[15] P. Bai, D.A. Cogswell, M.Z. Bazant, Nano Lett. 11 (11) (2011) 4890–4896.
[16] T.R. Ferguson, M.Z. Bazant, J. Electrochem. Soc. 159 (12) (2012) A1967–A1985.
[17] I.V. Thorat, T. Joshi, K. Zaghib, J.N. Harb, D.R. Wheeler, J. Electrochem. Soc. 158 (11) (2011) A1185–A1193.
[18] M. Farkhondeh, C. Delacourt, J. Electrochem. Soc. 159 (2) (2012) A177–A192.
[19] M. Safari, C. Delacourt, J. Electrochem. Soc. 158 (2) (2011a) A63–A73.
[20] K.E. Thomas-Alyea, ECS Trans. 16 (13).
[21] M. Safari, C. Delacourt, J. Electrochem. Soc. 158 (5) (2011b) A562–A571.
[22] P. Arora, R.E. White, M. Doyle, J. Electrochem. Soc. 145 (10) (1998) 3647–3667.
[23] J. Vetter, P. Novak, M.R. Wagner, C. Veit, K.C. Moller, J.O. Besenhard, M. Winter, M. Wohlfahrt-Mehrens, C. Vogler, A. Hammaouche, J. Power Sources 147 (2005) 269–281.
[24] R. Darling, J. Newman, J. Electrochem. Soc. 145 (3) (1998) 990–997.
[25] M. Safari, M. Morcrette, A. Teyssot, C. Delacourt, J. Electrochem. Soc. 156 (3) (2009) A145–A153.
[26] P. Ramadass, B. Haran, R. White, B.N. Popov, J. Power Sources 123 (2003) 230–240.
[27] G. Ning, B.N. Popov, J. Electrochem. Soc. 151 (10) (2004) A1584–A1591.
[28] R.P. Ramasamy, J.W. Lee, B.N. Popov, J. Power Sources 166 (2007) 266–272.
[29] M. Safari, C. Delacourt, J. Electrochem. Soc. 158 (12) (2011c) A1436–A1447.
[30] V.R. Subramanian, V.D. Diwakar, D. Tapriyal, J. Electrochem. Soc. 152 (10) (2005) A2002–A2008.
[31] T.S. Dao, C.P. Vyasarayani, J. McPhee, J. Power Sources 198 (2012) 329–337.
[32] N. Baba, H. Yoshida, M. Nagaoka, C. Okuda, S. Kawauchi, J. Power Sources 252 (2014) 214–228.
[33] V.R. Subramanian, V. Boovaragavan, V. Ramadesigan, M. Arabandi, J. Electrochem. Soc. 156 (4) (2009) A260–A271.
[34] K.A. Smith, C.D. Rahn, C.Y. Wang, J. Dyn. Syst. Trans. ASME 130 (2008) 011012.
[35] L. Cai, R.E. White, J. Electrochem. Soc. 156 (3) (2009) A154–A161.
[36] V.S. Kumar, J. Power Sources 222 (2013) 426–441.
[37] V.S. Kumar, P. Gambhire, K.S. Hariharan, A. Khandelwal, S.M. Kolake, D. Oh, S. Doo, J. Power Sources 248 (2014) 383–387.
[38] Y. Ye, Y. Shi, A.A.O. Tay, J. Power Sources 217 (2012) 509–518.
[39] M. Safari, C. Delacourt, J. Electrochem. Soc. 158 (10) (2011d) A1123–A1135.
[40] V. Srinivasan, J. Newman, Electrochem. Solid-State Lett. 9 (3) (2006) A110–A114.
[41] M. Broussely, S. Herreyre, P. Biensan, P. Kasztejna, K. Nechev, R.J. Staniewicz, J. Power Sources 97–98 (2001) 13–21.